ORIGINAL PAPER



High-pressure crystal structure and equation of state of ferromagnesian jeffbenite: implications for stability in the transition zone and uppermost lower mantle

Fei Wang¹ • Elizabeth C. Thompson² • Dongzhou Zhang³ • Ercan E. Alp⁴ • Jiyong Zhao⁴ • Joseph R. Smyth⁵ • Steven D. Jacobsen¹

Received: 6 May 2021 / Accepted: 28 September 2021 © The Author(s), under exclusive licence to Springer-Verlag GmbH Germany, part of Springer Nature 2021

Abstract

Jeffbenite, ideally Mg₃Al₂Si₃O₁₂, has been identified as inclusions in super-deep diamonds originating from depths that exceed 300 km. Although Mg-end member jeffbenite has limited stability at upper-mantle conditions, iron-bearing jeffbenite may have broader P-T stability that extends to the transition zone or uppermost lower mantle, incorporating significant amounts of ferric iron. Using synchrotron-based, single-crystal X-ray diffraction (XRD) and synchrotron Mössbauer spectroscopy (SMS) at pressures up to 29 GPa, we report the crystal structure, compressibility, and likely spin transition of iron in ferromagnesian jeffbenite ($Mg_{2.32}Al_{0.03}Fe^{2+}_{1.28}Fe^{3+}_{1.77}Si_{2.85}O_{12}$). High-pressure structure refinements reveal that Fe^{3+} substitution for Si in the T2 site, which shares edges with the M2 octahedron, likely stabilizes jeffbenite at high pressure, because it increases the cation-to-cation distance between these sites. Although ferromagnesian jeffbenite does not undergo a structural phase transition below 30 GPa, SMS hyperfine parameters suggest the onset of an electronic spin transition of iron from high-spin (HS) to low-spin (LS) at around 22 GPa, which may increase its stability at high pressures. Pressure-volume data were fit to a third order Birch–Murnaghan equation of state, resulting in $V_0 = 816.54(9)$, $K_{70} = 181.54(1.39)$, and $K'_{70} = 816.54(9)$ 2.76(14). These equation of state parameters are applicable to evaluating the encapsulation pressures of super-deep diamonds. The density and bulk modulus of ferromagnesian jeffbenite are similar to or higher than pyrope-almandine, pyrope-majorite, and skiagite-majorite solid solution garnets, further suggesting that jeffbenite may be an important ferric-iron silicate in the deeper parts of the mantle transition zone and uppermost lower mantle. However, future studies on the influence of temperature and oxidation state on the stability and equations of state of iron-bearing jeffbennite are still needed to determine what role, if any, jeffbenite plays in transition-zone mineralogy.

Keywords Jeffbenite · Transition zone · Ferric iron · Equation of state · Mössbauer · High pressure

Communicated by Dante Canil.

- Fei Wang feiwang2020@u.northwestern.edu
- Department of Earth and Planetary Sciences, Northwestern University, Evanston, IL 60208, USA
- Department of Earth and Environmental Systems, Sewanee: The University of the South, Sewanee, TN 37375, USA
- ³ Hawai'i Institute of Geophysics and Planetology, School of Ocean and Earth Science and Technology, University of Hawai'i at Manoa, Honolulu, HI 96822, USA
- Advanced Photon Source, Argonne National Laboratory, Argonne, IL 60439, USA
- Department of Geological Sciences, University of Colorado, Boulder, CO 80309, USA

Introduction

The tetragonal almandine—pyrope phase (TAPP), recently established as the mineral jeffbenite (Nestola et al. 2016), was first discovered as an inclusion in a diamond from São Luiz, Mato Grosso state, Brazil (Harris et al. 1997). As its original moniker suggests, jeffbenite is tetragonal and has a chemical formula very close to that of almandine—pyrope; however, the structure is more similar to zircon than to garnet, with two tetrahedral sites, two octahedral sites and one distinct capped tetrahedral site with $8 (2 \times 4)$ -coordinated coordination (Fig. 1). A structural formula for jeffbenite can be written as $(M1)_1(M2)_2(M3)_2(T1)_1(T2)_2(O1)_4(O2)_4(O3)_4$, with Mg-dominated M1 and M3 sites, Si-dominated T1 and T2 sites, and Al at the M2 sites (Harris et al. 1997; Finger

 $\underline{\underline{\mathscr{D}}}$ Springer

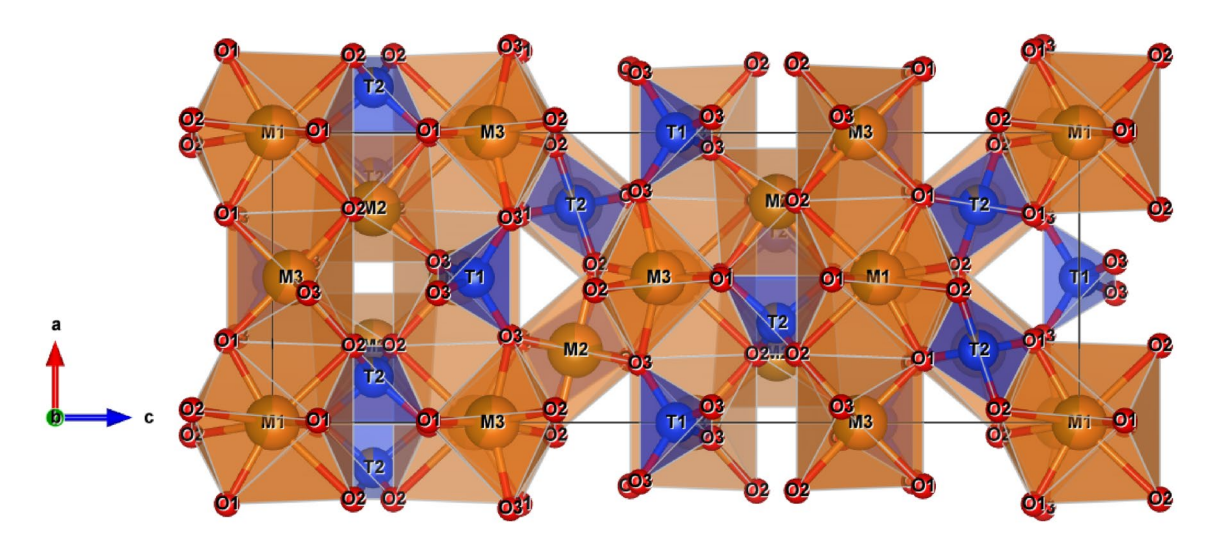


Fig. 1 Crystal structure of Fe-rich jeffbenite at 29 GPa projected onto the b-axis, drawn using VESTA (Momma and Izumi 2011). Silicate tetrahedra are colored blue and labeled T1 and T2. Octahedral sites

M1, M2, and M3 are occupied by Fe and Mg and colored orange. The structure is a tetragonal orthosilicate, more similar to that of zircon than garnet due to the body centered symmetry

and Conrad 2000; Nestola et al. 2016). After its initial discovery, jeffbenite was found as inclusions in several additional diamonds from Brazil's Juina district (Hutchison et al. 2001; Hayman et al. 2005; Bulanova et al. 2010; Zedgenizov et al. 2014, 2020) as well as in a diamond from Kankan in Guinea (Brenker et al. 2002). Laboratory synthesis of jeffbenite has only been reported twice. Armstrong and Walter (2012) synthesized low-iron jeffbenite at pressures of 6–10 GPa and temperatures of 1600–2000 K using a laser heated diamond anvil cell. More recently, Smyth et al. (2021) reported the synthesis of an iron-rich jeffbenite using a multi-anvil apparatus at 15 GPa and 1473 K, from which the samples in this study derive.

There is considerable debate regarding whether jeffbenite inclusions in diamond represent a primary phase from the transition zone or uppermost lower mantle, or a retrograde phase formed during ascent. The first identified sample of jeffbenite was found co-existing with ferropericlase, bridgmanite, and calcium silicate perovskite, suggesting an origin in the lower mantle (Harte and Harris 1994; Harris et al. 1997). Mössbauer spectra of that first sample indicated that jeffbenite contains high amounts of ferric iron, consistent with bridgmanite, supporting the hypothesis that it formed in the lower mantle (McCammon et al. 1997). Since then, jeffbenite has been reported in several different mineral assemblages in diamond, mostly composed of phases stable near the boundary of the transition zone and lower mantle (Hutchison et al. 2001; Hayman et al. 2005; Bulanova et al. 2010; Zedgenizov et al. 2014, 2020). Based on this evidence, Harte (2010) proposed that the close association of jeffbenite with ferropericlase and bridgmanite may indicate that jeffbenite replaces majoritic garnet in the bottom part of the mantle transition zone or uppermost lower mantle.

Conversely, Finger and Conrad (2000) argued that jeffbenite is a retrograde phase that forms during the ascent of the host diamond based on a three-pronged argument that: (1) jeffbenite has a lower density (3.580 g·cm⁻³) compared to the density of garnets with similar composition $(3.634 \text{ g}\cdot\text{cm}^{-3})$ (Harris et al. 1997), (2) jeffbenite has low cation coordination numbers compared with known lower mantle minerals, and (3) the T2 tetrahedron and M2 octahedron in jeffbenite are edge-sharing and, therefore, may be unstable at high pressure owing to the proximity of Si⁴⁺ and Mg²⁺ in those sites. Finger and Conrad (2000) further argued that the volume ratio of these two sites, the edgesharing T2 site and M2 octahedron, is too small for jeffbenite to be a high-pressure phase. The theory that jeffbenite is a retrograde phase was also supported by Brenker et al. (2002), who reported jeffbenite intergrown with olivine in contact with diopside, which the authors interpreted as evidence of jeffbenite formed from the breakdown of ringwoodite. However, Brenker et al. (2002) also suggested that a high Fe³⁺ content could stabilize the jeffbenite structure in the uppermost lower mantle.

Until recently, the only study to examine the stability field of jeffbenite concluded that jeffbenite is not stable at pressure–temperature (P–T) conditions exceeding 13 GPa and 1700 K (Armstrong and Walter, 2012). However, this study evaluated Ti-bearing and low-Fe jeffbenite, whereas a subsequent study by Anzolini et al. (2016) found that the absence of TiO₂ can extend the stability field of jeffbenite to higher P–T conditions. Nestola et al. (2016) suggested that jeffbenite should be classified based on the Ti and Fe composition, and that because the stability of jeffbenite is compositionally dependent the Fe-end member analogue of jeffbenite may be an important constituent in the Earth's



interior. The recent synthesis of ferric—iron rich, ferromagnesian jeffbenite supports the interpretation that increased iron-content increases the P–T stability of jeffbenite (Smyth et al. 2021). Based on these results, Fe-rich, low-Ti jeffbenite is potentially stable at the P–T conditions of the lower transition zone.

Importantly, evaluating the role of mixed-valence iron in extending the thermodynamic stability of jeffbenite has not been carried out. The identification of natural Fe-rich jeffbenite diamond inclusions (e.g., Bulanova et al. 2010; Thomson et al. 2014) within super-deep diamonds that originate from depths exceeding 300 km highlights the importance that iron substitution may play a role in extending the stability field of jeffbenite in the deep Earth. Based on these naturally occurring diamond inclusions, a systematic examination of the influence of iron, specifically ferric iron substitution, on the structure, stability and elastic properties of jeffbenite at the pressures of the deep mantle is needed to delimit the stability of jeffbenite in the Earth's interior.

Here we use synchrotron-based, single-crystal X-ray diffraction (XRD) and synchrotron Mössbauer spectroscopy (SMS) up to a maximum pressure of 29 GPa to investigate the crystal structure, compressibility, and magnetic properties of ferromagnesian jeffbenite, $Mg_{2.32}Al_{0.03}Fe^{2+}_{1.28}Fe^{3+}_{1.77}Si_{2.85}O_{12}$. Single-crystal structure refinements provide a detailed picture of how the structure of Fe-bearing jeffbenite evolves as a function of pressure, providing important constraints on the extent to which ferric iron occupancy in the tetrahedral T2 site sharing an edge with M2 sites influences the high-pressure stability of this phase. In addition, we have determined the equation of state of jeffbenite, which is applicable to determining the encapsulation pressures of jeffbenite diamond inclusions. Time-domain synchrotron Mössbauer spectroscopy (SMS) was used to measure the electronic environment of the iron atoms as a function of pressure, showing the likely onset of a spin-pairing transition of iron, which may further increase the stability-depth of jeffbenite in the deep mantle.

Materials and methods

Single crystals of Al-free, ferromagnesian jeffbenite measuring up to 200 µm in largest dimension were synthesized from a mixed oxide powders of FeO, Fe₂O₃, SiO₂, MgO and Mg(OH)₂ in a multi-anvil press at 15 GPa and 1473 K at Bayerisches Geoinstitut, University of Bayreuth, Germany (Smyth et al. 2021). Although synthesized in a hydrous environment, both IR and Raman spectroscopy show that the jeffbenite crystals are anhydrous (Smyth et al. 2021). Electron microprobe chemical analyses were performed using a JEOL 8230 electron microprobe at the University of Colorado, resulting in a chemical composition of 34.39 wt%

SiO₂, 0.31 Al₂O₃, 18.63 wt% MgO, and 44.23 wt% FeO. Synchrotron Mössbauer spectroscopy (MS) measurements result in a Fe³⁺/SFe value of 58(1)% and indicate that the M2 site is likely dominated by Fe³⁺, while the Fe²⁺ cations are concentrated in the M1 and M3 sites. Using the value of SFe/(SFe+Mg)=0.57 from the EMPA data and the Fe³⁺/ SFe=0.58 from SMS, the formula of this jeffbenite can be represented by $Mg_{2.32}Al_{0.03}Fe^{2+}_{1.28}Fe^{3+}_{1.77}Si_{2.85}O_{12}$. A complete characterization of the synthesized material used in this study can be found in Smyth et al. (2021).

High-pressure single-crystal X-ray diffraction measurements were carried out using a short-symmetric diamond anvil cells (DAC) with 78° apertures. To minimize systematic errors, P-V and structural data were collected on two different samples, each loaded into separate DACs. The first sample used 400 µm culet Boehler-Almax diamond anvils and the second sample used 300 µm culet Boehler-Almax diamond anvils. Sample chambers of 250 µm and 180 µm diameter, respectively, were laser ablated into rhenium sample gaskets pre-indented to ~40 µm thickness. Ferromagnesian jeffebenite single crystals were polished on both sides to produce samples of near uniform thickness (10 µm). These polished grains were loaded into the DACs, alongside a ~ 10 µm diameter ruby sphere, which was used as the pressure standard using the quasi-hydrostatic calibration of the R1 luminescence line from Jacobsen et al. (2008). Neon was loaded as the pressure-transmitting medium (Rivers et al. 2008).

Ambient pressure and high-pressure single-crystal XRD measurements were conducted using the six-circle diffractometer on the 13-BM-C beamline of the Advanced Photon Source (APS), Argonne National Laboratory. The incident X-ray beam uses a silicon (311) crystal as a monochromator to produce radiation with a wavelength of 0.434 Å and 1 eV energy bandwidth, which was focused to a $15 \times 15 \,\mu\text{m}^2$ spot. A Pilatus 1 M (Dectris) detector with a 1 mm thick silicon sensor was used to collect the diffraction patterns. The alignment of the detector was calibrated using LaB₆ (Zhang et al. 2017). A gas membrane system was used to increase the pressure of the samples remotely. Step-scan exposures were collected at two different detector positions 20 degrees apart in 2θ angle with an exposure time of 1 s/deg at each pressure point. Diffraction intensity data of jeffbenite at ambient conditions (1-bar) were collected prior to gas loading, and at each subsequent pressure step after gas loading to enable a crystal structure refinement at regularly increasing pressure steps.

Diffraction data and unit cell parameters were analyzed using the APEX3 software (Bruker). The SHELXL software was run on an Olex2 general user interface (Sheldrick, 2008; Dolomanov et al. 2009) to refine the crystal structure using peak intensities from the APEX3 data analysis. The starting crystal structure model used that of Smyth et al. (2021),

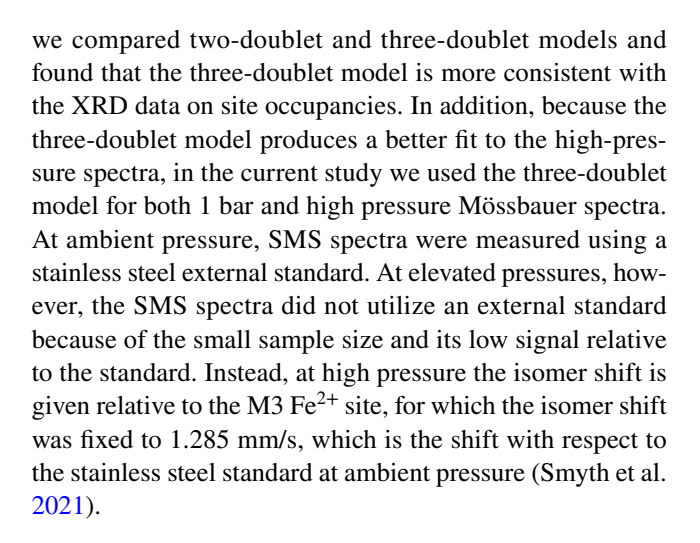


setting the T1 site as fully occupied by Si, and the T2 site fully occupied by a mixture of Si and Fe, with Si having 94% site occupancy. The M1, M2, and M3 sites were set as fully occupied by a mixture of Mg and Fe, with Mg on 60%, 36% and 65% of these sites, respectively. Cations occupying the same site have the same fractional coordinates and the same isotropic displacement parameters, but the ratio of the elements was allowed to vary when this value was first fit to data from our sample at ambient condition. Once the 1-bar ratios were fit, these values were fixed at their ambient condition values for subsequent high-pressure structure refinements. The Pymatgen Python library (Ong et al. 2013) and Uncertainties Python library (Leibigot 2014) were used to calculate polyhedral volumes and bond lengths.

For the SMS measurements, high pressures were achieved using a short-symmetric DAC fit with 300 μ m diamond anvils. A 180 μ m diameter hole was laser ablated in a rhenium gasket pre-indented to ~70 μ m thickness to produce the sample chamber. A single crystal of jeffbenite measuring ~50 μ m thick was loaded into the DAC alongside a 10 μ m ruby sphere, which served as the pressure calibrant. As with the XRD experiments, neon was loaded as the quasi-hydrostatic pressure medium (Rivers et al. 2008).

Time domain synchrotron Mössbauer spectroscopy (SMS) was conducted at the beamline 3-ID-B of the APS. A combination of a Si (111) double crystal monochromator and a 4-bounce inline high-resolution monochromator was used to reduce the X-ray photon energy bandwidth to 1 meV at 14.4125 keV, which was then focused into a beam 15 µm in diameter using a Kirkpatrick-Baez type mirror. The APS storage ring was filled with 24 equally spaced electron bunches emitting X-ray pulses with time interval of 153 ns. The nuclear resonant delayed signal from ⁵⁷Fe isotope was recorded in the 28-128 ns time window after each X-ray pulse excitation. SMS data were collected at 8.6, 12.6, 21.2, and 28.9 GPa. The mean pressure drift during each SMS measurement was 0.7 GPa, as determined from ruby fluorescence measurement taken before and after each spectrum was collected.

Time domain spectra were fit using version 2.2.0 of the CONUSS software (Sturhahn 2000) to obtain the hyperfine parameters of iron and the ferric-to-ferrous ratio in the sample. The starting model used in this study was recently published in Smyth et al. (2021). The SMS spectra for our ferromagnesian jeffbenite sample at ambient conditions could be fit to either a three doublet model with one high spin Fe³⁺ site and two high spin Fe²⁺ sites or a two doublet model with one high spin Fe³⁺ site and one high spin Fe²⁺ site. At ambient pressure the two doublet model produced a statistically better fit, whereas at high pressures (> 1-bar) the three doublet model with the additional Fe²⁺ site produces a statistically better fit. In a previous study on the synthesis and characterization of this material (Smyth et al., 2021)



Results

Lattice parameters

Over our experimental pressure range (0–29 GPa), we observed no phase transitions or abrupt change in lattice parameters. The lattice parameters at each pressure step are given in Tables 1S and 2S. Using the unit-cell volumes, our data were fit to a third-order Birch–Murnaghan equation of state (B–M EOS):

$$P(V) = \frac{3K_{T0}}{2} \left[\left(\frac{V_0}{V} \right)^{\frac{7}{3}} - \left(\frac{V_0}{V} \right)^{\frac{5}{3}} \right] \left\{ 1 + \frac{3}{4} \left(K_{T0} - 4 \right) \left[\left(\frac{V_0}{V} \right)^{\frac{2}{3}} - 1 \right] \right\},$$

where K_{T0} is the bulk modulus at ambient pressure, K'_{T0} is the first pressure derivative of the bulk modulus at ambient pressure, and V_0 is the unit-cell volume at ambient pressure. The EOS fit was performed with EOSFit7c using an error-weighted least squares fit (Angel et al. 2014; Gonzalez-Platas et al. 2016).

The resulting EOS parameters, as well as parameters resulting from a fit to a second-order B-M EOS, are reported in Table 1. The two samples produced the same result within mutual uncertainties for the second-order B-M EOS. The EOS parameters from a fit to a combined data set from both samples are $V_0 = 816.87(14)$, $K_{T0} = 171.66(0.85)$, $K'_{T0} = 4$ (fixed) for the second-order B–M EOS and $V_0 = 816.54(9)$, $K_{T0} = 181.54(1.39), K'_{T0} = 2.76(14)$ for the third-order B-M EOS. The pressure–volume (P-V) data are shown in Fig. 2 alongside the third-order B-M EOS fit to the combined data from both samples. To better visualize the quality of the EOS fit, a plot of normalized stress, $F_E = P/3f_E(1+2f_E)^{(5/2)}$, versus Eulerian strain, $f_E = ((V_0/V)^{(2/3)} - 1)/2$, is provided in the inset of Fig. 2. As shown in Fig. 2 inset, the negative slope of the $F_E - f_E$ plot illustrates a K'_{T0} value less than 4, consistent with our third order B-M EOS parameters. In



Sample 1

Sample 2

a/a0

c/c0

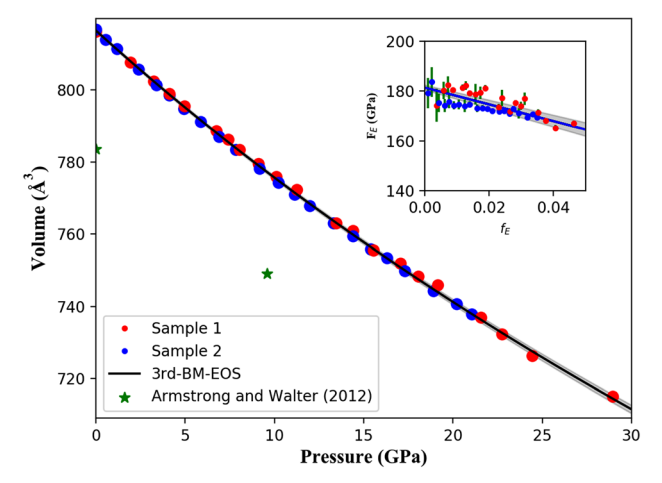
Table 1 Birch—Murnaghan EOS parameters for ferromagnesian jeffbenite fitted using refined lattice parameters from single crystal XRD measurements

$\rho_0 (g^* cm^{-3})$	$V_0 (\mathring{A}^3)$	K ₀ (GPa)	K'_{T0}	Sample	Refs	
3.871	816.87 (14)	171.67 (85)	4 (fixed)	Combined jeffbenite data	This study	
3.873	816.54 (9)	181.54 (1.4)	2.76 (14)			
3.871	816.96 (30)	172.7 (1.8)	4 (fixed)	Jeffbenite sample 1	This study	
3.874	816.24 (13)	187.92 (1.6)	2.31 (14)			
3.872	816.82 (5)	170.67 (41)	4 (fixed)	Jeffbenite sample 2	This study	
3.782	816.70 (5)	174.8 (1.1)	3.43 (13)			
4.325	1528.62	185 (3)	4.2	Almandine (Fe ₃ Al ₂ Si ₃ O ₁₂)	Zhang et al. (1999)	
3.563	1502.9 (3)	171 (2)	4.4 (2)	Pyrope (Mg ₃ Al ₂ Si ₃ O ₁₂)	Zhang et al. (1998)	
4.578	1611.8 (3)	157.4 (3.0)	5.7 (1.2)	Skiagite (Fe ₃ Fe ₂ Si ₃ O ₁₂)	Woodland and Ross (1994)	
3.525	1513.1	161	4	Majorite (Mg ₄ Si ₄ O ₁₂)	Yagi et al. (1992)	
3.678	1574.14(4)	173 (1)	4	Majoritic garnet	Nishihara et al. (2005)	

1.00

0.94

0.92 0.90



Normalized lattice parameters 0.88 V/V0 0.86 10 15 20 25 Pressure (GPa) Fig. 3 Pressure dependence of normalized unit cell parameters, a/a_0 ,

Fig. 2 Pressure-volume data of two Fe-rich jeffbenite samples. Red and blue symbols differentiate samples that were loaded into separate DACs. Volume data of low-iron jeffbenite from Armstrong and Walter (2012) are also plotted for comparation. The black solid curve is the third-order B-M EOS fit to the combined data set and the grey shaded region is the 95% prediction band. The inset shows normalized stress versus Eulerian strain $(F_E - f_E)$, where the reference volume (V_0) from the third-order B—M EOS was used

addition, the reduction of misfit by adding a free parameter of K'_{T0} to describe the pressure derivative of the bulk modulus is significant at the 99% confidence level, based on an F test. However, because K_0 and K_0 ' are inversely correlated, systematic errors in the lattice parameters would affect both parameters.

Axial compression data, which are normalized to the ambient pressure data, are plotted in Fig. 3. To determine the compressibility of the a- and c-axes in jeffbenite, a linearized second-order B-M EOS fit was used, where each axial dimension was cubed and treated as volume in the Birch-Murnaghan formulation (Angel et al. 2014;

 c/c_0 and V/V_0 . The black solid curves are the third-order B—M EOS fit to the combined data set of sample 1 and sample 2, and the grey shaded regions show 95% prediction bands

Gonzalez-Platas et al. 2016). The linear modulus (linear incompressibility), defined as $M_{l0} = (\beta_{l0})^{-1}$, where the reference linear compressibility evaluated at P = 0is $\beta_{10} = l^{-1}(\delta l/\delta P)_{P=0}$, describes how the linear dimension l changes with pressure. As the two samples produce the same result within mutual uncertainties, we fit the combined data from both samples. The linear moduli for the a- and c-axes are 701.3(4.2) and 323.6(3.5) GPa, respectively, which correspond to normalized, nondimensional axial compressibility values of $1.423(9) \times 10^{-3}$ and $3.13(4) \times 10^{-3}$. There is considerable anisotropy in the axial compressibility, as the ratio between the a- and c-axes at ambient pressure is 1:0.45, meaning the c-axis is about twice as compressible as the a-axis. The structural data at high pressure, given below, suggests this is due to the large compressibility of the O3–O3 interatomic



distances of the M2 octahedron, which are nearly parallel to the c-axis.

Structure refinements

The jeffbenite structure contains two distinct octahedral sites (M2 and M3) and one 8 (2×4)-coordinated capped tetrahedral site (M1) occupied by Fe³⁺, Fe²⁺ or Mg²⁺, two distinct Si⁴⁺ tetrahedral sites (T1 and T2) and three oxygen positions (Fig. 1). From the previous characterization (Smyth et al. 2021), it is likely that M1 and M3 contain most of the Fe²⁺, while M2 contains Fe³⁺. We also note significant substitution for Si by Fe³⁺ in T2 (Smyth et al. 2021). The edge sharing of the divalent octahedra leaves little room for cation-oxygen-cation angles to bend, motivating analysis of the jeffbenite structure in terms of the component cation-oxygen polyhedra. Of the three M sites, Smyth et al. (2021) pointed out that the M1 cation is analogous to the Zr position in zircon but with reduced symmetry. As such, there are four additional oxygen atoms located near to the M1 site with bond lengths of 2.139(6) Å at ambient pressure, and four oxygen atoms with longer bond lengths of 2.570(7) Å. Both of these M1–O bonds have a similar compressibility: the four longer M1-O2 bonds have a compressibility of 0.00184(10) GPa⁻¹, while the four shorter M1–O1 bonds have a compressibility of 0.00159(8) GPa⁻¹. The corresponding bulk modulus for the M1 polyhedron is 155.6(8.7) GPa. M1–O distance and M1 polyhedron volume versus pressure are shown in Fig. 4A and Fig. 1S. Within the M3 octahedral site, the M3–O2 bonds have a compressibility of 0.00214(10) GPa⁻¹ compared to 0.00193(10) GPa⁻¹ and 0.00199(12) GPa⁻¹ for the M3–O1 and M3–O3 bonds, respectively. The corresponding M3 polyhedron's bulk modulus is 122.8(4.3) GPa, as shown in Fig. 4D and Fig. 1S.

The M2 polyhedron is the least compressible of the three M sites, with a bulk modulus of 183.3(7.4) GPa. The longest M2-O1 bonds and the second longest M2-O2 bonds have similar linear compressibilities of 0.00155(8) GPa⁻¹ and 0.00189(10) GPa⁻¹, respectively, but the shortest M2–O3 bonds do not exhibit linear compressibility. Rather, the length of the M2–O3 bonds are relatively stable at ~ 1.94 Å until 6 GPa, at which point they decrease to ~ 1.90 Å from 6 to 12 GPa, and then again remained unchanged up to 29 GPa (Fig. 4B). This anomalous behavior might be linked to the decrease of the O3-M2-O3 angle with pressure. This angle at ambient pressure is 102° but by 29 GPa this angle is decreased to 92°. As a result, the O3–O3 distance decreases quite dramatically with pressure. In fact, the compressibility of the O3–O3 distance, which is nearly parallel to the c-axis, is slightly larger than that of the c-axis. In addition, due to

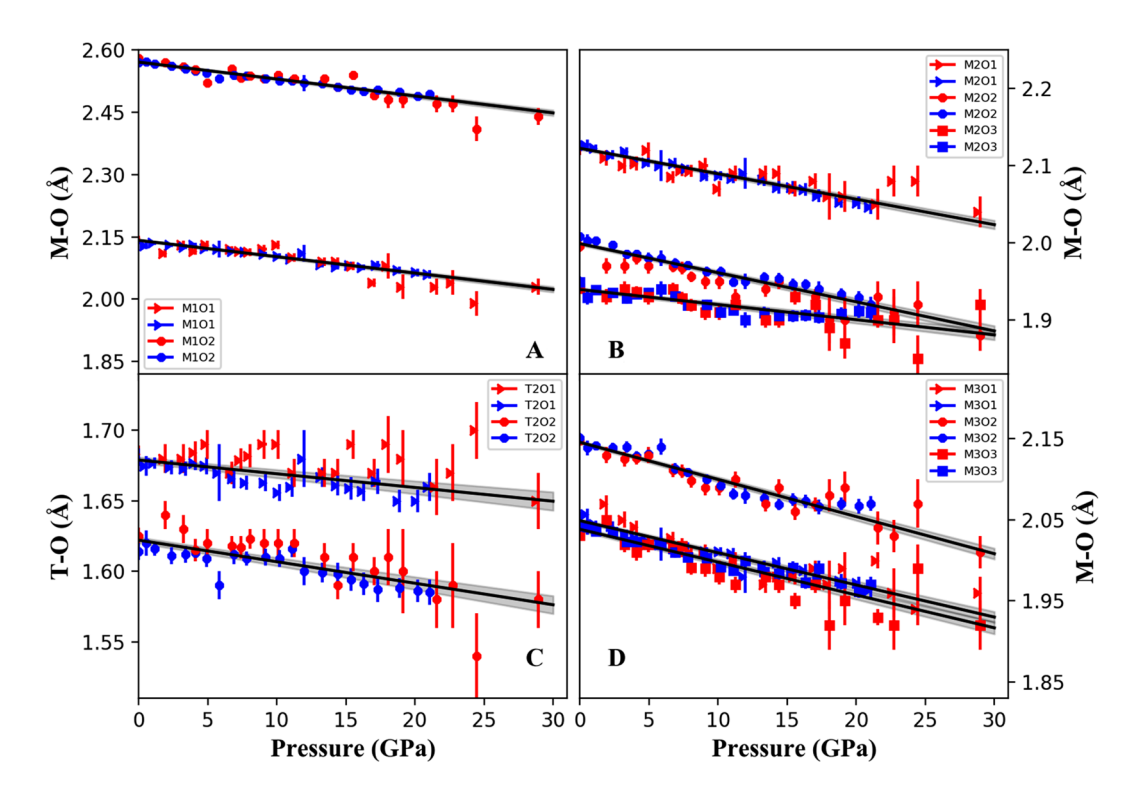


Fig. 4 Pressure dependence of polyhedral bond lengths in Fe-bearing jeffbenite, including (A) M1 capped tetrahedral site (M1O $_8$), (B) M2 octahedral site (M2O $_6$), (C) T2 tetrahedral site (T2O $_4$), and (D) M3 octahedral site (M3O $_6$). Red (sample 1) and blue (sample 2) colors

distinguish the replicate samples of this study. The black solid curves show second-order B—M EOS fits to the combined data set and the grey shaded regions show the 95% prediction band



the decrease of the O3–M2–O3 angle, the bond angle variance of the M2 octahedron decreases.

Both T1 and T2 tetrahedra exhibit similar compressibilities, with bulk moduli of 200(50) and 237(30) GPa for T1 and T2, respectively. However, at high pressure, the behavior of these tetrahedra differs. T2 shares an edge with the M2 octahedron and, therefore, does not have three-dimensional linkage, and the T2-O1 and T2-O2 bonds have compressibilities of 0.00058(12) GPa⁻¹ and 0.00094(12) GPa⁻¹, respectively (Fig. 4C). The T1 tetrahedron has only one type of T1–O bond, with a compressibility of 0.00102(14) GPa⁻¹. The T1 tetrahedron does not share an edge or face with any other polyhedron but is connected to the M2 and M3 octahedra by a shared corner. At elevated pressure, both the M2-O3-T1 and M3-O3-T1 angles change by about 5 degrees (Fig. 5). Since the M2 and M3 octahedra are connected by a shared O2-O3 edge, these two angle changes are likely correlated.

Mössbauer spectroscopy

Synchrotron Mössbauer spectroscopy (SMS) measurements were made at ambient temperature and pressures of 1 bar, 8.6 GPa, 12.6 GPa, 21.2 GPa, and 28.9 GPa. The measured time domain spectra and calculated energy domain spectra of the best-fit hyperfine models from these experiments are shown in Fig. 6. Best-fit hyperfine parameters (quadruple splitting and isomer shifts) are provided in Table 2 and plotted in Fig. 7. The isomer shifts reported in Table 2 are relative values obtained with the M3 isomer shift fixed at the 1-bar value of 1.285 mm/s. Since the relative isomer shift of the two other sites (M1 and M2) were fit with respect

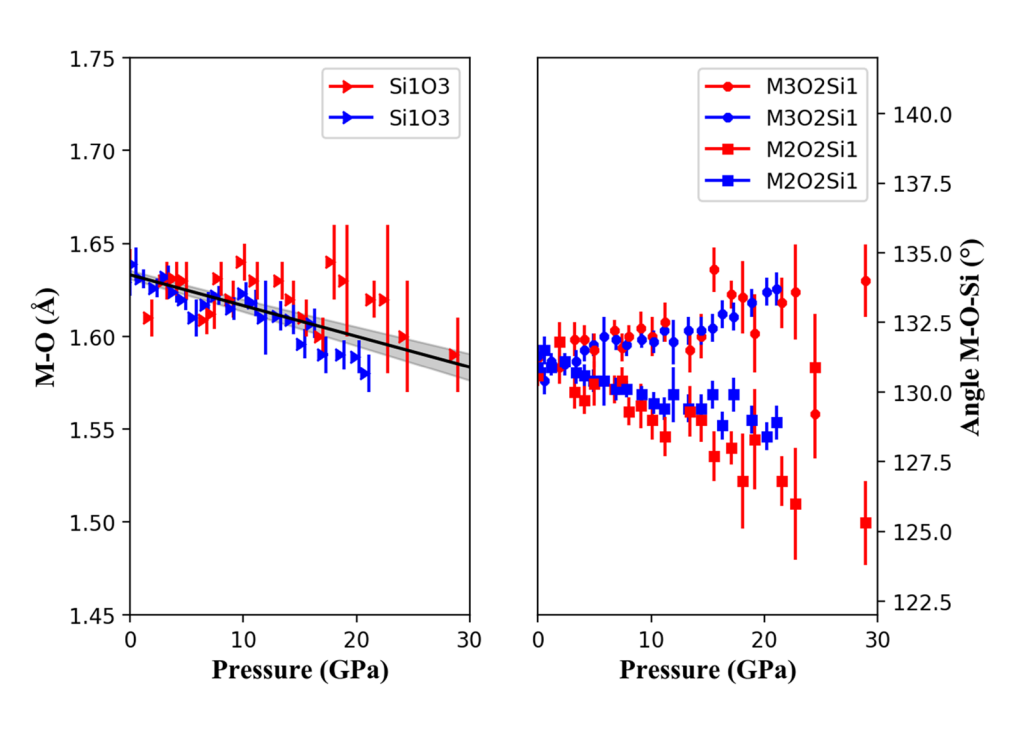
to the M3 site, these should not be interpreted as absolute isomer shifts.

The ambient pressure SMS data show that 58(1)% of the total atomic percent iron is Fe³⁺ with an isomer shift of 0.578(3) mm/s and quadrupole splitting of 0.581(2) mm/s (Smyth et al. 2021). Each of the two Fe²⁺ sites have a similar proportion, and their isomer shifts are 1.285 mm/s and 1.11(1) mm/s and the quadrupole splitting are 1.751(6) mm/s and 2.632(9) mm/s, respectively. With increased pressure, the SMS spectra changed but by very little up to 22 GPa. with only the quadrupole splitting of the M2 site decreasing slightly with pressure. However, at the highest pressure evaluated (28.9 GPa), the spectra changed significantly, with the emergence of a new feature near 80 ns. A four doublet model was evaluated as a potential model for the 28.9 GPa spectra, but the three doublet model used at intermediate pressure provided a higher quality fit to the data. The 28.9 GPa SMS data reveal a significant increase in the isomer shifts of the M1 and M2 sites with respect to the M3 site.

Discussion

Until now, the only estimate of the bulk modulus of jeffbenite was made by Nestola et al. (2016), who used two data points from the diffraction data of Armstrong and Walter (2012) and the relationship of $K_{T0} = \Delta P/(\Delta V/V_0)$, resulting in a value of 218 GPa. This bulk modulus is unexpectedly high, being about 46 GPa (or 27%) higher than the value we obtained for Fe-bearing jeffbenite. Although one might expect there to be some compositional dependence with the addition of iron, the large difference between

Fig. 5 Pressure dependence of the T1—O3 bond and the angle between M2(3)—O3—T1 in Ferich jeffbenite. Red (sample 1) and blue (sample 2) colors distinguish the replicate samples of this study. The black solid curve is the second-order B—M EOS fit to the combined data set and the grey shaded region shows the 95% prediction band





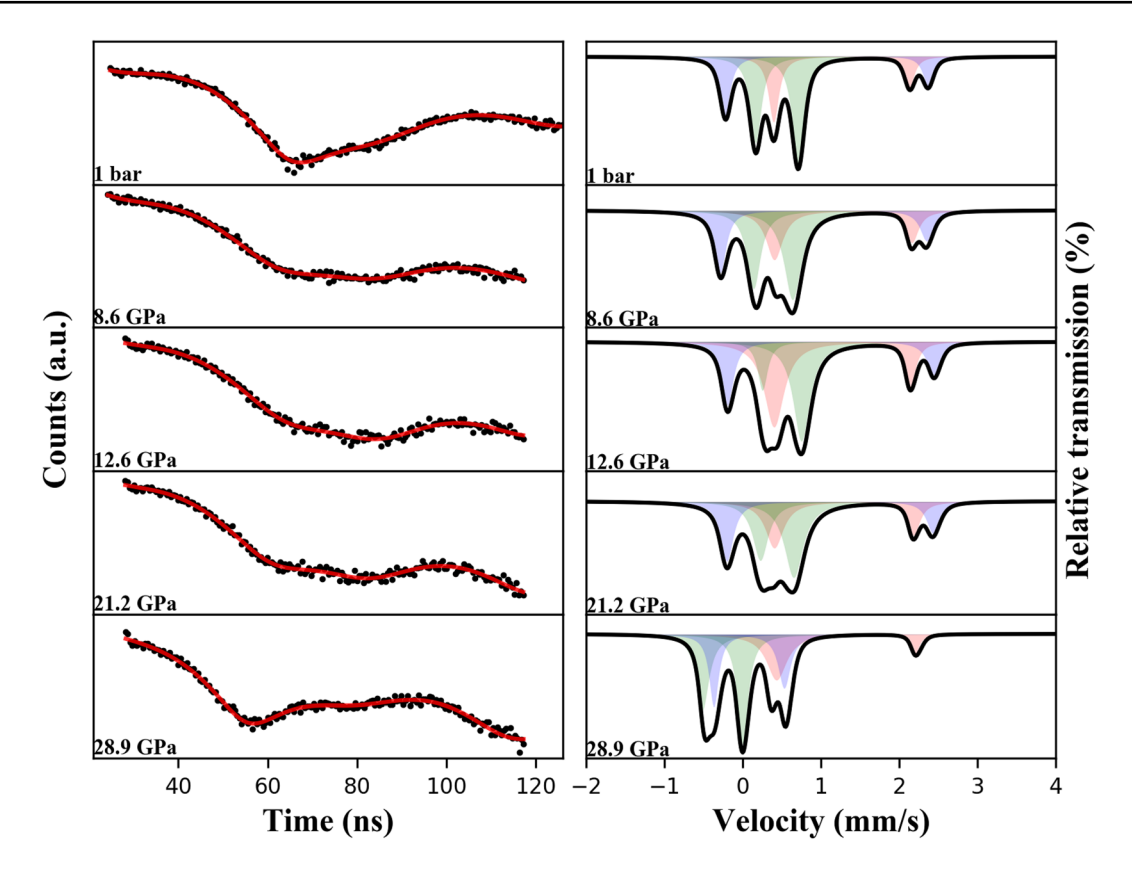


Fig. 6 SMS time domain spectra (left panel) and simulated energy spectra (right panel) of Fe-bearing jeffbenite at ambient pressure and high pressure. The ambient pressure spectra are from our previous

study (Smyth et al. 2021). The shaded blue and red peaks are the four ${\rm Fe^{2+}}$ peaks and the shaded green peaks are the two ${\rm Fe^{3+}}$ peaks

Table 2 Best-fit hyperfine parameters of the SMS spectra. The isomer shift of the M3 site was fixed at 1.285 mm/s and the weight of the M3 sub-lattice was fixed at 0.1

Pressure	Effective thickness	M3	M2			M1		
		Quadrupole splitting	Weight of the sub- lattice	Isomer shift	Quadrupole splitting	Weight of sub- lattice	Isomer shift	Quadrupole splitting
1 bar	17.8 (3)	1.751 (6)	0.22 (2)	0.47 (1)	0.560 (7)	0.077 (7)	1.11 (1)	2.632 (9)
8.6 GPa	43 (2)	1.75 (1)	0.37 (5)	0.39 (4)	0.48 (2)	0.09(1)	1.04(4)	2.69(2)
12.6 GPa	47 (2)	1.728 (8)	0.32 (5)	0.47 (4)	0.45(2)	0.073 (7)	1.12(2)	2.68 (3)
21.2 GPa	62.4 (4)	1.80(2)	0.48 (6)	0.42(1)	0.378 (8)	0.12(1)	1.10(1)	2.67(1)
28.9 GPa	15.6 (3)	1.70(2)	0.32 (4)	-0.27(1)	0.483 (5)	0.19(3)	0.077 (5)	0.92(2)

the previous estimate and our determination of the bulk modulus is more likely due to the fact that Nestola et al. (2016) used only two data points and a linear fit over the pressure range of 0–9.6 GPa, skewing the bulk modulus to higher values than would be obtained using data over an expanded pressure range or with high-density data at lower pressures. Nevertheless, considering jeffbenite is a Mg–Fe solid solution, it is important for future work to evaluate the EOS of Mg–jeffbenite using high-density

pressure-volume data as we have done for ferromagnesian jeffbenite.

A summary of compressibility data for jeffbenite compared with garnets is given in Table 1. The bulk modulus of jeffbenite $(\text{Fe}^{2+},\text{Mg})_2(\text{Fe}^{3+},\text{Mg})_3\text{Si}_3\text{O}_{12}$ in this study of 182(2) GPa is higher than that of pyrope with $K_{T0}=171(2)$ GPa (Zhang et al. 1999) and comparable to almandine with $K_{T0}=185(3)$ GPa (Zhang et al. 1999). The pressure derivative obtained by Zhang et al. (1999) for pyrope–almandine



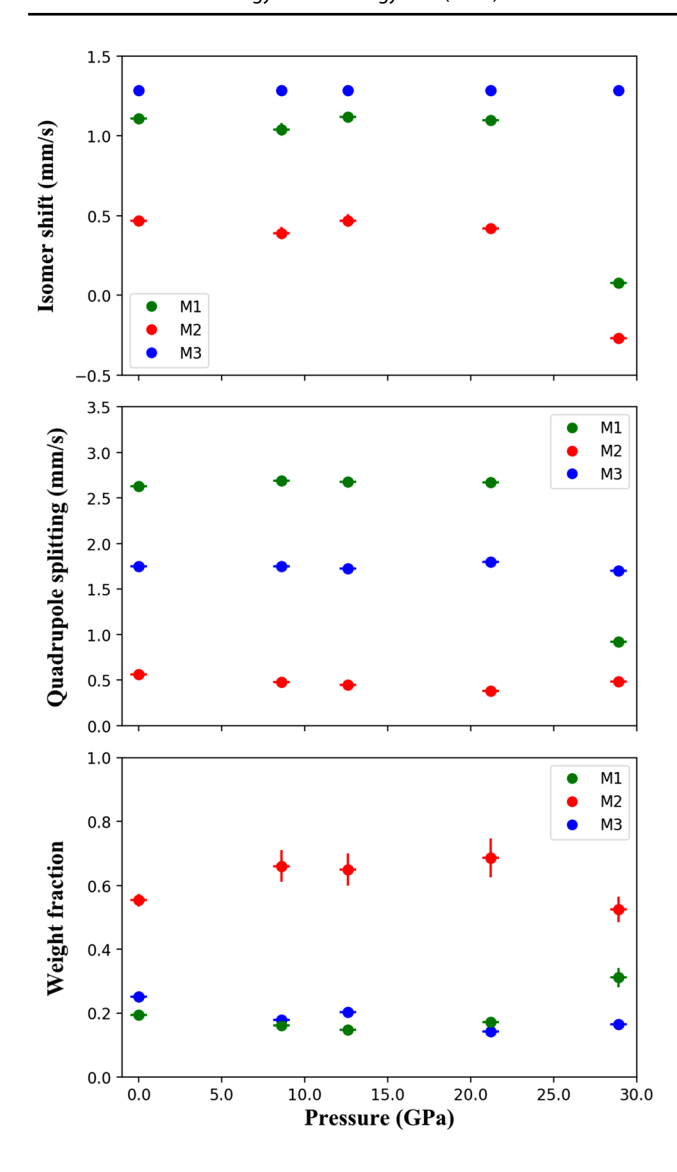


Fig. 7 Fitted SMS hyperfine parameters (isomer shift and quadrupole splitting) and weight fraction of the iron sites of jeffbenite as a function of pressure

garnets, however, is $K'_{T0} = 4.0$ –4.2, so a more direct comparison is our value of $K_{T0} = 172(1)$ GPa with K'_{T0} fixed at 4, which is about the same as pyrope and about 7% lower than almandine. Our value for the bulk modulus of jeffbenite using the second-order B–M EOS fit ($K'_{T0} = 4$) of 172(1) GPa is also the same as majoritic garnet with mid-ocean ridge basalt (MORB) composition, with $K_{T0} = 173(1)$ and $K'_{T0} = 4$ (Nishihara et al. 2005), however, if we compare using our third-order B–M EOS fit with $K_{T0} = 182(1)$, our jeffbenite is about 5% less compressible than MORB-composition majorite. The compressibility of skiagite (Fe₃Fe₂Si₃O₁₂) and majorite (Mg₄Si₄O₁₂) solid solution was studied by Ismailova et al. (2017) and for skiagite components ranging from 24 to 76%, the bulk moduli range from 157 to 172 GPa (Ismailova et al. 2017), which suggests that jeffbenite is less compressible

than iron-rich majoritic garnet. The high bulk modulus of jeffbenite relative to majoritic garnet further suggests that it may well be a stable phase in the lower transition zone and uppermost lower mantle. Our value of $K'_{T0} = 2.76(14)$ for jeffbenite is considerably lower than has been fit in EOS data for most garnets (Table 1). The relatively high bulk modulus and lower (best fit) pressure derivative determined in this study for Fe-bearing jeffbenite indicates that it can be a favorable phase in this compositional space at the pressures of the mantle transition zone and uppermost lower mantle.

Lower mantle minerals typically have higher densities than crustal and upper mantle minerals and have structures containing sites with large coordination numbers (Irifune and Tsuchiya, 2007). Ferromagnesian jeffbenite in this study has a calculated density of 3.87 g·cm⁻³ at ambient conditions, and is comparable to garnets with similar compositions (Table 1). Because the bulk modulus is the same as or higher than comparable garnets (Table 1) and has a best-fit lower pressure derivative, it is likely that the density of jeffbenite will remain comparable or become higher than pyrope-almandine or majoritic garnets at deep mantle conditions. Previous work by Harte (2010) indicated that jeffbenite may replace majoritic garnet in the lower mantle transition zone or upper lower mantle. Smyth et al. (2021) further showed that ferromagnesian jeffbenite may be a stable phase in the mantle transition zone, where it may replace garnet in the transition zone if the transition zone is rich in aluminum and/or ferric iron.

Conversely, the jeffbenite structure differs significantly from the garnet structure (Smyth et al. 2021) and as shown by this study, the high-pressure structural evolution of ferromagnesian jeffbenite is also distinct. In garnets, early work (e.g., Hazen et al. 1994) suggested that structural evolution at high pressure is dominated by the octahedral and tetrahedral framework. More recent work by Zhang et al. (1998) on the other hand, found that the structural adaptation of garnets to high pressure is dominated by kinking of the Si-O-M angle. However, these two mechanisms (polyhedral framework vs. kinking bond angle) may be correlated, as Zhang et al. (1998) used a linear relationship between normalized Si-O-Al kinking angle and normalized distortion parameters of MgO₈ and AlO₆ polyhedra to argue that kinking is the dominant factor in structural change. In jeffbenite, we find that although there was a change with pressure in the Si-O-M2(M3) kinking angle, there is no corresponding large change in the distortion parameters of the M3 octahedron. If kinking is the dominant mechanism for structural adaptation to high pressure in jeffbenite, it is unlikely that only the bond angle of the M2 octahedron changed, while the M3 octahedron distortion indices remained almost unchanged. Therefore, we argue that in jeffbenite Si-O-M2(M3) kinking is not the dominating factor in determining structural adaptation to high pressure,



but rather that the angle change is itself due to the unequal compressibility of the three M polyhedra.

In our evaluation of the evolution of the structure of Alfree ferromagnesian jeffbenite at high pressure, we note that the "capped tetrahedra site" (M1), two octahedral sites (M2 and M3), and two tetrahedra T sites comprise, respectively, 10.44%, 10.55%, 9.95%, 1.08% and 2.19% of the unit cell volume at ambient pressure. The bulk modulus of jeffbenite can be calculated using the bulk moduli of the constituent polyhedra weighted by their volume fraction producing a Voigt average of 171 GPa. In addition, the Reuss average was calculated as 168 GPa (Watt et al. 1976 and references therein). These Voigt and Reuss averages are very similar to the bulk modulus value obtained by fitting our V-P data to a second-order B–M EOS (172 GPa). It is not usually possible to simply correlate the macroscopic bulk moduli with the bulk moduli of the constituent polyhedral in the unit cell, as polyhedral linkages and the compression of non-polyhedral volume can contribute significantly to the bulk moduli (Hazen and Finger, 1979). In our study, the fact that the B-M EOS bulk modulus is nearly identical to the bulk modulus determined using the moduli of the constituent polyhedra indicates that the compression of jeffbenite is mainly accommodated by polyhedral compression. In jeffbenite, the M1 capped tetrahedron and the M2 and M3 octahedra are the most compressible units and, therefore, accommodate most of the compression of the unit cell at elevated pressures.

The individual octahedral bonds are unlikely to contribute significantly to the anisotropic compression of jeffbenite. All the M–O bonds, except M2–O3 and M2–O1, exhibit similar compressibilities, and since both the M2–O3 and M2–O1 bonds are almost parallel to the diagonal between the a- and c-axes, it is also unlikely that they contribute to the anisotropic compression of jeffbenite. That the O3–O3 distances have almost the same compressibility as the c-axis, and that this distance is almost parallel to the c-axis, suggest that the M2 octahedral compressibility, especially the large compressibility of the O3–O3 distances of the M2 octahedron, might be the main contribution to the anisotropic compression of jeffbenite.

Finger and Conrad (2000) argued that the volume ratio of the edge-sharing M2 site and T2 site is too small for jeffbenite to be a stable high-pressure phase. This early study evaluated the first jeffbenite sample found, which had an average M2/T2 bond length ratio of 1.17—significantly smaller than the 1.225–1.235 ratio now considered typical. It is possible that the small volume ratio of Finger and Conrad (2000) is due to M2 occupancy by Al and Cr. The M2/T2 ratio of our sample is 1.227, which is a reasonable ratio for a high-pressure phase. In our ferromagnesian sample, there are Fe³⁺ cations at the T2 sites, which may help to explain why our ratio is higher than that reported by Finger and Conrad (2000) and also explains how iron, especially Fe³⁺, stabilizes jeffbenite

at high pressure. The T2–M2 (cation-to-cation) distance in our sample is 2.775 Å, which is significantly larger than the T2–M2 distance (2.6747 Å) in the sample reported by Finger and Conrad (2000). Even at pressure higher than 20 GPa, the T2–M2 distance in our sample is still longer than that of aluminum-bearing Mg–jeffbenite from Finger and Conrad (2000) at ambient pressure (Fig. 8). Therefore, the incorporation of Fe³⁺ likely controls the expanded pressure-stability of ferromagnesian jeffbenite over Mg–jeffbenite.

Between 22 and 29 GPa, we observe changes in the hyperfine parameters that indicate that one of the high spin Fe²⁺ sites changes into an Fe³⁺-like site. Although we do not observe a discontinuous reduction in the unit-cell volume or lattice parameters over this pressure range, there is a concurrent reduction in the M1 volume. The changes in hyperfine parameters and M1 volume suggest that high-spin (HS) ferrous iron undergoes a spin transition an intermediate or low-spin (LS) state. Although 22-29 GPa would be a relatively low pressure for the onset of a spin transition compared to (Mg,Fe)O, recent studies report that a HS to mixed (HS+LS) or intermediate spin transition state of Fe²⁺in bridgmanite initiates at or below 30 GPa (McCammon et al. 2008; Mao et al. 2015). A pressure range of ~30 GPa for the onset of HS to HS+LS states is also comparable to the transition pressure in Fe³⁺-bearing δ -(Al,Fe) OOH (30 GPa) (e.g., Hsieh et al. 2020), γ-FeOOH (35 GPa) (Reagan et al. 2016), and ferric iron in the NAL phase (30 GPa) (Wu et al. 2016). Future X-ray emission spectroscopy experiments should explore the high-pressure spin states of mixed-valence iron in ferromagnesian jeffbenite further. We

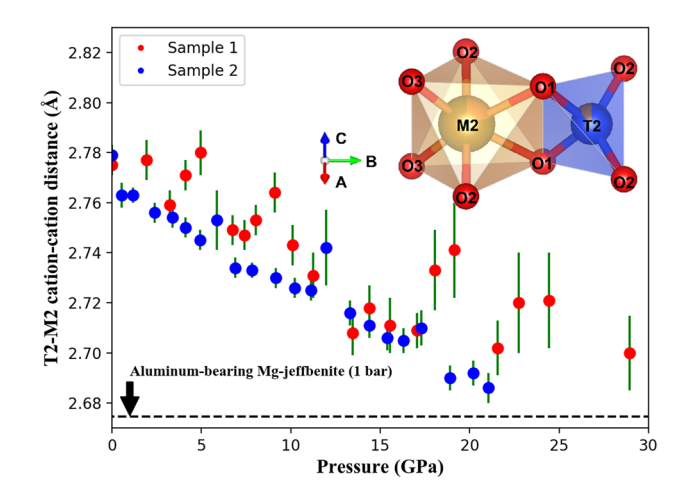


Fig. 8 T2—M2 cation—cation distances versus pressure for ferromagnesian jeffbenite, wherein both Si and Fe³⁺ occupy T2. The black dashed line shows the T2—M2 distance of an aluminum-bearing Mg—jeffbenite from Finger and Conrad (2000) at ambient pressure (2.6747A), where both Si and Al occupy T2. The inset shows the local structure of the edge-sharing M2 octahedral site and T2 tetrahedral site. Occupancy of T2 with Fe³⁺ increases T2—M2, stabilizing the structure to higher pressures



should note that the isomer shift of -0.27 mm/sec for M2 site is given relative to the ambient pressure isomer shift value of the M3 site, so it is not an absolute value, but it is a value pegged to the M3 site.

Knowledge of the pressure–temperature stability of jeffbenite relative to garnet and majoritic garnet requires further study to ascertain its importance in the Earth's mantle. The somewhat common occurrence of jeffbenite as inclusions in diamonds (Nestola et al. 2016; Harris et al. 1997; Brenker et al. 2002; Hutchison et al. 2001; Kaminsky, 2012; Hayman et al. 2005; Bulanova et al. 2010; Zedgenizov et al. 2014, 2015, 2020) has led to competing theories with synthesis experiments that indicate jeffbenite may be part of the stable phase assemblage (Hutchison et al. 2001; Hayman et al. 2005; Bulanova et al. 2010; Zedgenizov et al. 2014, 2020). Although in-situ volume data on jeffbenite still included in diamond have not been reported, using the equation of state data determined in this paper, it may be possible to estimate entrapment pressures using the elastic geobarometry approach (Angel et al. 2017), which has been applied to other diamond inclusions, such as ferropericlase (Anzolini et al. 2019), magnesiochromite (Nestola et al. 2019) and olivine (Nestola et al. 2011). Ideally, the effects of iron substitution for Mg and temperature should be explored in the future to improve geobarometry using jeffbenite inclusions in diamond.

Although this compression study was performed at room temperature, some preliminary statements about how temperature affects the stability of jeffbenite can be made from previous observations. First, since the sample was synthesized at 15 GPa and 1473 K and it coexisted with primitive clinopyroxene, it is likely that there is a true stability field for iron-rich jeffbenite near 450 km depth under oxidizing and iron rich conditions for certain bulk compositions (Smyth et al. 2021). Second, since iron-rich jeffbenite has been identified as a diamond inclusion within a diamond that likely originated from the boundary between the mantle transition zone and lower mantle (Bulanova et al. 2010), the stability field for iron-rich jeffbenite may extend to even lower than 450 km depth. In the future, a semi-empirical thermodynamic phase equilibria calculation could be used to evaluate the stability of iron-bearing jeffbenite once a more complete set of thermodynamic parameters becomes available. In this work, we contribute the 300 K reference equation of state, but future work at high-temperature remains necessary to calculate phase equilibria.

Conclusions

The high-pressure crystal structure, magnetic structure, and equation of state of Al-free ferromagnesian jeffbenite was determined by synchrotron-based, single-crystal XRD and SMS at pressures up to 29 GPa. No phase changes or abrupt

changes in lattice parameters were observed in this pressure interval. Based on a rigorous analysis of the structural adaptation of ferromagnesian jeffbenite to elevated pressures, our study supports the finding that iron-substitution stabilizes jeffbenite at high pressure by reducing the cation-cation repulsion between the shared-edge sites of T2 and M2. At 29 GPa, the T2-M2 cation distance in ferromagnesian jeffbenite is still longer than it is in Mg-jeffbenite at room pressure. The increase of the M2/T2 ratio in ferromagnesian jeffbenite refutes concerns that this phase is unstable at the pressures of the lower transition zone and uppermost lower mantle. Based on our high-pressure findings, coupled with the increased thermodynamic stability due to increased Fecontent described by Smyth et al. (2021), and the observation of natural Fe-rich jeffbenite diamond inclusions (e.g., Bulanova et al. 2010; Thomson et al. 2014), we argue that Fe-rich jeffbenite diamond inclusions were formed as a primary phase in the transition zone or uppermost lower mantle.

In our study, refined lattice parameters of ferromagnesian jeffbenite were used to obtain equation of state parameters for second- and third-order Birch–Murnaghan equations of state. The density and compressibility of ferromagnesian jeffbenite from this study are similar to the physical and chemical properties of pyrope–almandine solid solution garnets and larger than that of Fe-rich majoritic garnet. The change in hyperfine parameters between 22 and 29 GPa for the ferromagnesian jeffbenite indicates the initiation of a HS to intermediate or LS configuration.

Acknowledgements This research was supported by grants from National Science Foundation (NSF) EAR-1853521 to S.D. Jacobsen and EAR-1725673 to E.C. Thompson. This work was performed at Sector 3 and Sector 13 of the Advanced Photon Source (APS) at Argonne National Laboratory. GeoSoilEnviroCARS (Sector 13) is supported by the National Science Foundation – Earth Sciences (EAR – 1634415) and Department of Energy - GeoSciences (DE-FG02-94ER14466). This research used resources of the Advanced Photon Source, a U.S. Department of Energy (DOE) Office of Science User Facility operated for the DOE Office of Science by Argonne National Laboratory under Contract No. DE-AC02-06CH11357. Use of the COMPRES-GSECARS gas loading system was supported by COMPRES under NSF Cooperative Agreement EAR-1606856. Single-crystal diffraction experiments on beamline 13-BM-C were supported in part by the Partnership for Extreme Crystallography (PX^2) under NSF EAR-1661511. We thank Sergey Tkachev for help with gas loading. We would like to thank two anonymous reviews for their helpful comments and Dante Canil for handling this paper.

Availability of data and material Cifs available at Mendeley (https://data.mendeley.com/datasets/gj6pgn3hgg/draft?a=9e56d6ae-a874-4ede-8180-d0f2b30e169d).

Declarations

Conflict of interest The authors declare no conflict of interest or personal relationships that could have appeared to influence the work reported in this paper.



References

- Angel RJ, Alvaro M, Gonzalez-Platas J (2014) Eosfit7c and a Fortran module (library) for equation of state calculations. Zeitschrift Für Kristallographie- Crystalline Materials 229(5):405–419. https://doi.org/10.1515/zkri-2013-1711
- Angel RJ, Mazzucchelli ML, Alvaro M, Nestola F (2017) EosFit-Pinc: A simple GUI for host-inclusion elastic thermobarometry. Am Mineral 102:1957–1960. https://doi.org/10.2138/ am-2017-6190
- Anzolini C, Nestola F, Mazzucchelli ML, Alvaro M, Nimis P, Gianese A, Morganti S, Marone F, Campione M, Hutchison MT, Harris JW (2019) Depth of diamond formation obtained from single periclase inclusions. Geol 47(3):219–222. https://doi.org/10.1130/G45605.1
- Anzolini C, Drewitt J, Lord OT, Walter MJ, Nestola F (2016) New Stability Field of Jeffbenite (ex-"TAPP"): Possibility of Super-Deep Origin. In AGU Fall Meeting Abstracts
- Armstrong LS, Walter MJ (2012) Tetragonal almandine pyrope phase (TAPP): retrograde Mg-perovskite from subducted oceanic crust? Eur J Mineral 24(4):587–597. https://doi.org/10.1127/0935-1221/2012/0024-2211
- Brenker FE, Stachel T, Harris JW (2002) Exhumation of lower mantle inclusions in diamond: ATEM investigation of retrograde phase transitions, reactions and exsolution. Earth Planet Sci Lett 198(1–2):1–9. https://doi.org/10.1016/S0012-821X(02)00514-9
- Bulanova GP, Walter MJ, Smith CB, Kohn SC, Armstrong LS, Blundy J, Gobbo L (2010) Mineral inclusions in sublithospheric diamonds from collier 4 kimberlite pipe, Juina, Brazil: subducted protoliths, carbonated melts and primary kimberlite magmatism. Contrib Mineral Petrol 160(4):489–510. https://doi.org/10.1007/s00410-010-0490-6
- Dolomanov OV, Bourhis LJ, Gildea RJ, Howard JA, Puschmann H (2009) OLEX2: a complete structure solution, refinement and analysis program. J Appl Crystallogr 42(2):339–341. https://doi.org/10.1107/S0021889808042726
- Finger LW, Conrad PG (2000) The crystal structure of "tetragonal almandine-pyrope phase" (TAPP): A reexamination. Am Mineral 85(11–12):1804–1807. https://doi.org/10.2138/am-2000-11-1224
- Gonzalez-Platas J, Alvaro M, Nestola F, Angel RJ (2016) Eosfit7-GUI: a new graphical user interface for equation of state calculations, analyses and teaching. J Appl Crystallogr 49(4):1377–1382. https://doi.org/10.1107/S1600576716008050
- Harris J, Hutchison MT, Hursthouse M, Light M, Harte B (1997) A new tetragonal silicate mineral occurring as inclusions in lower-mantle diamonds. Nature 387(6632):486
- Harte B (2010) Diamond formation in the deep mantle: the record of mineral inclusions and their distribution in relation to mantle dehydration zones. Mineral Mag 74(2):189–215. https://doi.org/ 10.1180/minmag.2010.074.2.189
- Harte B, Harris J (1994) Lower mantle mineral associations preserved in diamonds. Mineral Mag 58:384–385
- Hayman PC, Kopylova MG, Kaminsky FV (2005) Lower mantle diamonds from Rio Soriso (Juina area, Mato Grosso, Brazil). Contrib Mineral Petrol 149(4):430–445. https://doi.org/10.1007/ s00410-005-0657-8
- Hazen RM, Finger LW (1979) Bulk modulus—volume relationship for cation-anion polyhedra. J Geophys Res Solid Earth 84(B12):6723–6728. https://doi.org/10.1029/JB084iB12p06723
- Hazen RM, Downs RT, Conrad P, Finger LE, Gasparik T (1994) Comparative compressibilities of majorite-type garnets. Phys Chem Miner 21(5):344–349. https://doi.org/10.1007/BF00202099
- Hsieh WP, Ishii T, Chao KH, Tsuchiya J, Deschamps F, Ohtani E (2020) Spin transition of iron in δ-(Al, Fe)OOH induces thermal

- anomalies in Earth's lower mantle. Geophys Res Lett. https://doi.org/10.1029/2020GL087036
- Hutchison MT, Hursthouse M, Light M (2001) Mineral inclusions in diamonds: associations and chemical distinctions around the 670km discontinuity. Contrib Mineral Petrol 142(1):119–126. https:// doi.org/10.1007/s004100100279
- Irifune T, and Tsuchiya T (2007) Mineralogy of the Earth: Phase transitions and mineralogy of the lower mantle. Treatise on Geophysics 2nd edn, ed G Schubert (Amsterdam: Elsevier), 2:33–62
- Ismailova L, Bykov M, Bykova E, Bobrov A, Kupenko I, Cerantola V, Vasiukov D, Dubrovinskaia N, McCammon C, Hanfland M, Glazyrin K, Liermann HP, Chumakov A, Dubrovinsky L (2017) Effect of composition on compressibility of skiagite-Fe-majorite garnet. Am Mineral 102(1):184–191. https://doi.org/10.2138/am-2017-5856
- Jacobsen SD, Holl CM, Adams KA, Fischer RA, Martin ES, Bina CR et al (2008) Compression of single-crystal magnesium oxide to 118 GPa and a ruby pressure gauge for helium pressure media. Am Mineral 93(11–12):1823–1828. https://doi.org/10.2138/am. 2008.2988
- Kaminsky F (2012) Mineralogy of the lower mantle: A review of 'super-deep' mineral inclusions in diamond. Earth Sci Rev 110(1–4):127–147. https://doi.org/10.1016/j.earscirev.2011.10.005
- Leibigot EO (2014) A Python Package for Calculations with Uncertainties
- Mao Z, Lin JF, Yang J, Inoue T, Prakapenka VB (2015) Effects of the Fe³⁺ spin transition on the equation of state of bridgmanite. Geophys Res Lett 42(11):4335–4342. https://doi.org/10.1002/ 2015GL064400
- McCammon C, Hutchison M, Harris J (1997) Ferric iron content of mineral inclusions in diamonds from Sao Luiz: a view into the lower mantle. Science 278(5337):434–436. https://doi.org/10.1126/science.278.5337.434
- McCammon C, Kantor I, Narygina O, Rouquette J, Ponkratz U, Sergueev I et al (2008) Stable intermediate-spin ferrous iron in lower-mantle perovskite. Nat Geosci 1(10):684–687. https://doi.org/10.1038/ngeo309
- Momma K, Izumi F (2011) VESTA 3 for three-dimensional visualization of crystal, volumetric and morphology data. J Appl Crystallogr 44(6):1272–1276. https://doi.org/10.1107/S0021889811038970
- Nestola F, Nimis P, Ziberna L, Longo M, Marzoli A, Harris JW, Manghnani MH, Fedortchouk Y (2011) First crystal-structure determination of olivine in diamond: Composition and implications for provenance in the Earth's mantle. Earth Planet Sci Lett 305(1-2):249-255. https://doi.org/10.1016/j.epsl.2011.03.007
- Nestola F, Burnham AD, Peruzzo L, Tauro L, Alvaro M, Walter MJ, Gunter M, Anzolini C, Kohn SC (2016) Tetragonal almandinepyrope phase, TAPP: finally a name for it, the new mineral jeffbenite. Mineral Mag 80(7):1219–1232. https://doi.org/10.1180/ minmag.2016.080.059
- Nestola F, Zaffiro G, Mazzucchelli ML, Nimis P, Andreozzi GB, Periotto B, Princivalle F, Lenaz D, Secco L, Pasqualetto L, Logvinova AM (2019) Diamond-inclusion system recording old deep lithosphere conditions at Udachnaya (Siberia). Sci Rep 9(1):1–8. https://doi.org/10.1038/s41598-019-48778-x
- Nishihara Y, Aoki I, Takahashi E, Matsukage KN, Funakoshi KI (2005) Thermal equation of state of majorite with MORB composition. Phys Earth Planet Inter 148(1):73–84. https://doi.org/10.1016/j.pepi.2004.08.003
- Ong SP, Richards WD, Jain A, Hautier G, Kocher M, Cholia S, Ceder G (2013) Python materials genomics (pymatgen): A robust, open-source Python library for materials analysis. Comput Mater Sci 68:314–319. https://doi.org/10.1016/j.commatsci.2012.10.028



- Reagan MM, Gleason AE, Daemen L, Xiao Y, Mao WL (2016) Highpressure behavior of the polymorphs of FeOOH. Am Mineral 101(6):1483–1488. https://doi.org/10.2138/am-2016-5449
- Rivers M, Prakapenka VB, Kubo A, Pullins C, Holl CM, Jacobsen SD (2008) The COMPRES/GSECARS gas-loading system for diamond anvil cells at the advanced photon source. High Pressure Res 28(3):273–292
- Sheldrick GM (2008) A short history of SHELX. Acta Crystallogr A 64(1):112–122. https://doi.org/10.1107/S0108767307043930
- Smyth JR, Wang F, Alp EE, Bell AS, Posner ES, Jacobsen SD (2021) Ferromagnesian jeffbenite synthesized at 15 GPa and 1200 °C. Am Mineral. https://doi.org/10.2138/am-2021-7852
- Sturhahn W (2000) CONUSS and PHOENIX: Evaluation of nuclear resonant scattering data. Hyperfine Interact 125(1–4):149–172. https://doi.org/10.1023/A:1012681503686
- Thomson AR, Kohn S, Bulanova G, Smith C, Araujo D, Walter M et al (2014) Origin of sub-lithospheric diamonds from the Juina-5 kimberlite (Brazil): constraints from carbon isotopes and inclusion compositions. Contrib Mineral Petrol 168(6):1081. https://doi.org/10.1007/s00410-014-1081-8
- Watt JP, Davies GF, O'Connell RJ (1976) The elastic properties of composite materials. Rev Geophys 14(4):541–563. https://doi.org/ 10.1029/RG014i004p00541
- Woodland AB, Ross CR (1994) A crystallographic and mössbauer spectroscopy study of Fe₃²⁺Al₂Si₃O₁₂-Fe₃²⁺Fe₂³⁺Si₃O₁₂,(almandine-"skiagite") and Ca₃Fe₂³⁺Si₃O₁₂-Fe₃²⁺Fe₂³⁺Si₃O₁₂ (andradite-"skiagite") garnet solid solutions. Phys Chem Miner 21(3):117–132. https://doi.org/10.1007/BF00203142
- Wu Y, Wu X, Lin JF, McCammon CA, Xiao Y, Chow P, Prakapenka VB, Yoshino T, Zhai S, Oin S (2016) Spin transition of ferric

- iron in the NAL phase: Implications for the seismic heterogeneities of subducted slabs in the lower mantle. Earth Planet Sci Lett 434:91–100. https://doi.org/10.1016/j.epsl.2015.11.011
- Yagi T, Uchiyama Y, Akaogi M, Ito E (1992) Isothermal compression curve of MgSiO3 tetragonal garnet. Phys Earth Planet Inter 74(1–2):1–7. https://doi.org/10.1016/0031-9201(92)90063-2
- Zedgenizov D, Kagi H, Shatsky V, Ragozin A (2014) Local variations of carbon isotope composition in diamonds from São-Luis (Brazil): evidence for heterogenous carbon reservoir in sublithospheric mantle. Chem Geol 363:114–124. https://doi.org/10.1016/j.chemgeo.2013.10.033
- Zedgenizov D, Kagi H, Ohtani E, Tsujimori T, Komatsu K (2020) Retrograde phases of former bridgmanite inclusions in superdeep diamonds. Lithos 370:105659. https://doi.org/10.1016/j.lithos. 2020.105659
- Zhang L, Ahsbahs H, Kutoglu A (1998) Hydrostatic compression and crystal structure of pyrope to 33 GPa. Phys Chem Miner 25(4):301–307. https://doi.org/10.1007/s002690050118
- Zhang L, Ahsbahs H, Kutoglu A, Geiger C (1999) Single-crystal hydrostatic compression of synthetic pyrope, almandine, spessartine, grossular and andradite garnets at high pressures. Phys Chem Miner 27(1):52–58. https://doi.org/10.1007/s002690050240
- Zhang D, Dera PK, Eng PJ, Stubbs JE, Zhang JS, Prakapenka VB, Rivers ML (2017) High pressure single crystal diffraction at px². J Visualized Exp 119:e54660. https://doi.org/10.3791/54660

Publisher's Note Springer Nature remains neutral with regard to jurisdictional claims in published maps and institutional affiliations.

